Hindawi
International Journal of Antennas and Propagation
Volume 2019, Article ID 6262574, 11 pages
https://doi.org/10.1155/2019/6262574

Research Article

Nose-Cone Conformal Substrate-Integrated Waveguide Slot Array Antenna for X-Band Radar Applications

Hisham Khalil, M. Mansoor Ahmed, and Umair Rafique

Department of Electrical Engineering, Capital University of Science and Technology, Islamabad, Pakistan

Correspondence should be addressed to Umair Rafique; umairrafique.1987@gmail.com

Received 4 October 2019; Accepted 2 December 2019; Published 23 December 2019

Academic Editor: Chien-Jen Wang

This paper presents the design of nose-cone conformal substrate-integrated waveguide (SIW) slot array antenna for modern radar applications. Firstly, the wave propagation characteristics have been investigated in doubly curved SIW, and it has been observed that they are non-uniform along the longitudinal direction of nose-cone conformal SIW. To ensure the constant wave propagation along the length of conformal SIW, the conventional design of SIW is reformulated for nose-cone conformal SIW and circuit model modification has been demonstrated. Secondly, the procedure for designing a SIW-based array on curved surfaces has been developed. In the proposed design, rectangular waveguide (RWG) to SIW feeding structure has been used to avoid spurious radiations. Finally, 1×6 element-based nose-cone conformal slotted array has been designed and compared with planar and cylindrical conformal arrays. It has been observed from the results that the nose-cone conformal slot array offers low sidelobe levels (SLLs) and high gain. For the validation of the proposed design, the conformal slotted array has been fabricated and measured, which exhibited a reasonable agreement between the measured and the simulated data.

1. Introduction

In modern aircraft and unmanned aerial vehicles (UAVs), most of the communication systems depend on antennas. Generally, planar antenna arrays are utilized in these systems, which could potentially increase the payload and thus make the system inefficient [1]. To overcome these problems, now-a-days, conformal antennas are being used on the surface of aircraft and UAVs [2, 3]. Also, substrate-integrated waveguide (SIW) based conformal antennas are considered good candidates for airborne applications. SIW has the inherent property of the microstrip line with an added advantage of a waveguide. Moreover, it is compact in size and cost-effective and offers low insertion loss and better integration capability for microwave circuits compared with conventional waveguides [4–9]. The closed configuration of SIW suppresses the spurious radiations from feeding structure, which otherwise could lead to narrow beamwidth [4, 10].

In the literature, many conformal antenna arrays have been presented for multiple applications. In [11], a conformal Vivaldi antenna array with high gain and low sidelobe level (SLL) is presented for airborne applications. The array elements are synthesized using the Dolph-Chebyshev technique, and the presented array operates in the frequency range of 400–800 MHz. In [12], a conformal rectangular waveguide (RWG) is presented for aircraft applications. It covered 360° azimuth angle for scanning purpose in the frequency range of 16–16.6 GHz. However, the presented array is non-planar, which is considered a negative feature from the design perspective. In [13], a cylindrical conformal SIW-based traveling wave slot array is designed and implemented. The array consisted of 4×16 elements and employed microstrip to SIW type feeding structure conformed on a cylindrical surface. It was noted that this kind of configuration degrades radiation characteristics especially SLL. Another cylindrical conformal slotted array with large beam tilt (84°) is presented in [14]. The reported array had −13 dB SLL, but the design compromised over the beam scanning. A microstrip fed circular patch antenna array conformed on a cylinder for C-band applications is discussed in [15].

It is worth mentioning that the designs presented in [11–15] are simulation based and their experimental or analytical validation is not available. In [16], an analytical design approach is adopted and equations are presented for a cylindrical curved slot array. In [17], an experimental study for conformal antennas on aircraft surface is presented, wherein suitable material for array fabrication and their mechanical aspects are reported. Pelham et al. [18] estimated the gain of the conformal array on the wings of an aircraft and compared it with the gain of the conventional planar array. In [19], a conformal antenna array factor is simulated and optimized using a MATLAB program for radar scanning applications. The authors reported a peak SLL of −20 dB.

In the current state of conformal arrays, there is a need to investigate the integration of antenna arrays on the surface of high-speed jets. Owing to this, in this work, a nose-cone conformal SIW slotted array is designed, fabricated, and characterized at X-band. Since the conical surface is an essential part of aerodynamic applications such as space rockets, supersonic aircraft, and missiles [3]; therefore, design consideration of nose-cone conformal SIW is emphasized in this work. In cylindrical conformal SIW, the cross-section of SIW remains the same along longitudinal and circumferential directions; therefore, the wave propagation characteristics have to be uniform in the conformed structure. Thus, a standard slot array design procedure can be implemented on the cylindrical surface [20–24]. The same design strategy of a slot array cannot be implemented directly on doubly curved surfaces due to the involvement of θ and ϕ in the conformed SIW. Because of the variation in both θ and ϕ, the uniform wave propagation along the direction of nose-cone would be the first design challenge, while keeping the SLL at the desired level would be the second major consideration. In [25], a conical conformal SIW slot array antenna is presented for millimeter-wave applications. A flexible SIW transition from conical-to-cylindrical is designed for improved impedance matching. The presented configuration provides better return loss in the band of interest, but it has no effect on gain compared to its counterpart, i.e., conical surface. Furthermore, conical-to-cylindrical SIW transition can increase the size of the antenna structure, which limits its use in many aerodynamic applications.

In this paper, a design of the nose-cone conformal slot array antenna is presented for X-band radar applications. The problems in the wave propagation characteristics for such a medium are identified, and to overcome this issue, a generalized solution is proposed. It has also been demonstrated that the proposed design offers better performance compared with the design reported in [25]. Moreover, the proposed array is cost-effective and lightweight and offers enhanced radar coverage without involving mechanical steering. Furthermore, the conventional planar slot array needs protective radome for aircraft applications that implies dielectric losses [3], which are not there in the proposed design hence, making it a good candidate for such applications.

2. Characterization of SIW on Curved Surface

This section describes the wave propagation characteristics of conformal SIW on curved surfaces. Two curved surfaces are under consideration: cylindrical and conical. A planar SIW of width, W, and length, L, is conformed onto the cylinder of radius, r, along the longitudinal direction z as shown in Figure 1(a). The planar cross-sectional face of SIW is converted into a curved surface, and due to this change, the propagation constant, β, and input impedance, Z_{in}, will change. Since, the curvature of a cylindrical surface remains unchanged therefore, β will remain the same.

When planar SIW is conformed to the doubly curved surface such as nose-cone defined by spherical coordinates (r, ϕ, θ) as shown in Figure 1(b), to maintain the conformity, the cross-section of SIW will not remain the same along the height of the cone. In other words, the cross-sectional face of SIW is more conforming on the vertex of the cone as shown in Figure 1(b). This continuous structural variation causes a change in β. In this situation, the design of the slot array on SIW is not feasible as there could be $n^{\text{th}}\beta$ propagations on the surface of SIW. It means that every element on SIW will resonate at different β, and due to this phenomenon, the array cannot be analyzed practically.

To represent nose-cone conformal SIW in spherical coordinates, the base of excitation of SIW is at (r_1, ϕ_1, θ) and short circuit end is at (r_2, ϕ_2, θ)as shown in Figure 1(b). The cross-section at base has a radius r_1 at ϕ_1 and cross-section at vertex has a radius r_2 at ϕ_2. For wave propagation in conical SIW, the following condition must be validated [25, 26]:

$$r_1\phi_2 = r_2\phi_1. \tag{1}$$

On the other hand, the analytical expression for the change in β can be written as follows [26]:

$$\beta = \frac{u_{np}}{r_n}, \tag{2}$$

where u_{np} is the zeros of Bessel's function and r_n represents radii of the cone from base to vertex. If r_n changes, β also changes accordingly, and if r_n of a cone decreases or approaches towards zero, the corresponding ϕ increases according to equation (1) and consequently β increases as described in [25].

For slot array, it is assumed that n^{th} element is lying on any radius r_n. The mutual coupling between the array elements is difficult to establish and practically, the design is invalid for N number of elements. To overcome this problem, a design technique has been proposed whose explanation is provided in Section 3.

3. Modified Nose-Cone Conformal SIW

Two design topologies are presented for β regulation along the conformed surface: one is the cylindrical equivalent and other is the conical equivalent modification. Here, an assumption is made that at any location on the cone (L_n) as shown in Figure 2(a), one can consider that specific portion as a cylinder having radius according to the conical radius at

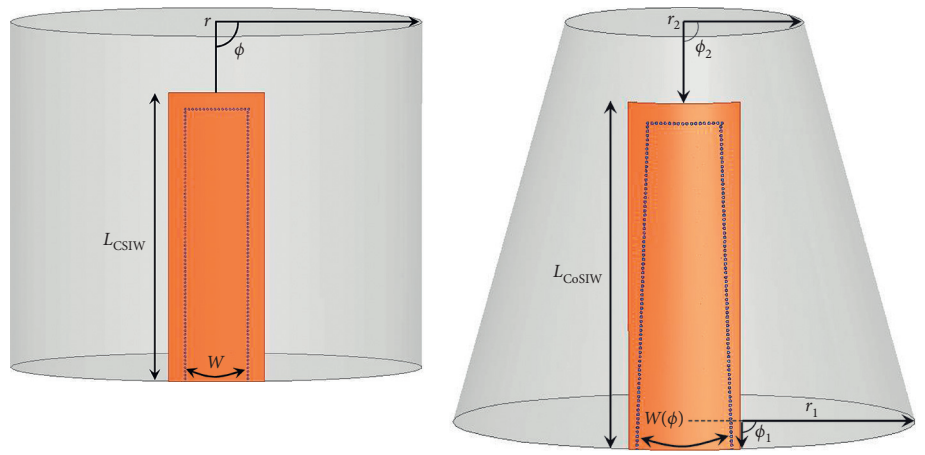

Figure 1: Conformal substrate-integrated waveguide on (a) cylindrical and (b) conical surfaces.

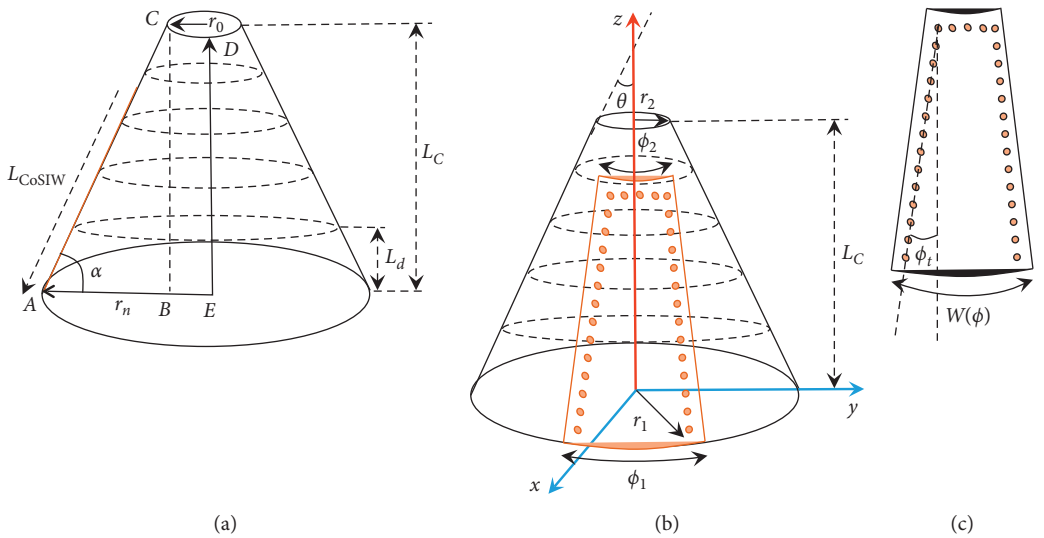

Figure 2: Cross-sectional view of nose-cone conformal SIW. (a) Side view. (b) Front view. (c) Tilted CoSIW.

that specific location defined by n. For this purpose, it is required to find the radius at the corresponding length L_C, which can be calculated as follows:

$$r_n - r_0 = L_n \times \cos(\alpha), \tag{3}$$

where

$$L_n = L_{CoSIW} - L_d. \tag{4}$$

As long as L_d sweeps from 0 to L_C, L_n traverses along the generatrix of nose-cone. In equation (4), L_{CoSIW} corresponds to the length of conformal SIW, which can be calculated through triangle ΔABC as shown in Figure 2(a). In the figure, the lines $\overline{AC} = L_{CoSIW}$, $\overline{BC} = L_C$, and $\overline{AB} = r_n - r_0$. By using Pythagoras theorem, L_{CoSIW} can be represented as follows:

$$L_{CoSIW} = \sqrt{(r_n - r_0)^2 + L_C^2}. \tag{5}$$

In equation (3), the variable α represents cone angle. A number of HFSS simulations of conformal SIW have been carried out for β_n curves against the tilted cylindrical conformed SIW, and the results are shown in Figure 3(a). One can observe from Figure 3(a) that the slope of β curves by increasing the value of L_C, as evident from Figure 2(b), is reducing. Examination of Figure 3(a) also shows that all the β_n curves are passing through a region labeled as area of interest. It is worth mentioning that all the β_n curves converge for a range of $\phi_t \sim 0.3^\circ - 0.5^\circ$. This range of ϕ_t provides unchanged β along the conformal SIW, thus for an appropriate design, a value of $\phi_t \approx 0.43^\circ$ has been selected, which gave $\beta = 230.5$ rad/m as marked area of interest in Figure 3(a).

In the second case, the geometrical structure has been modified, and now it is truly represented by a cone having bottom radius, r_1 and top radius, r_2 as shown in Figure 2(b). Series of simulations were performed by moving the probe from higher to the lower radius (r_1 to r_2), and the variation in β has been observed. It has been noted that, for $\phi_t \approx 0.43^\circ$ $\beta \approx 228$ rad/m is the value which is independent of L_C. Thus, this value is taken to calculate the length L_{CoSIW} of

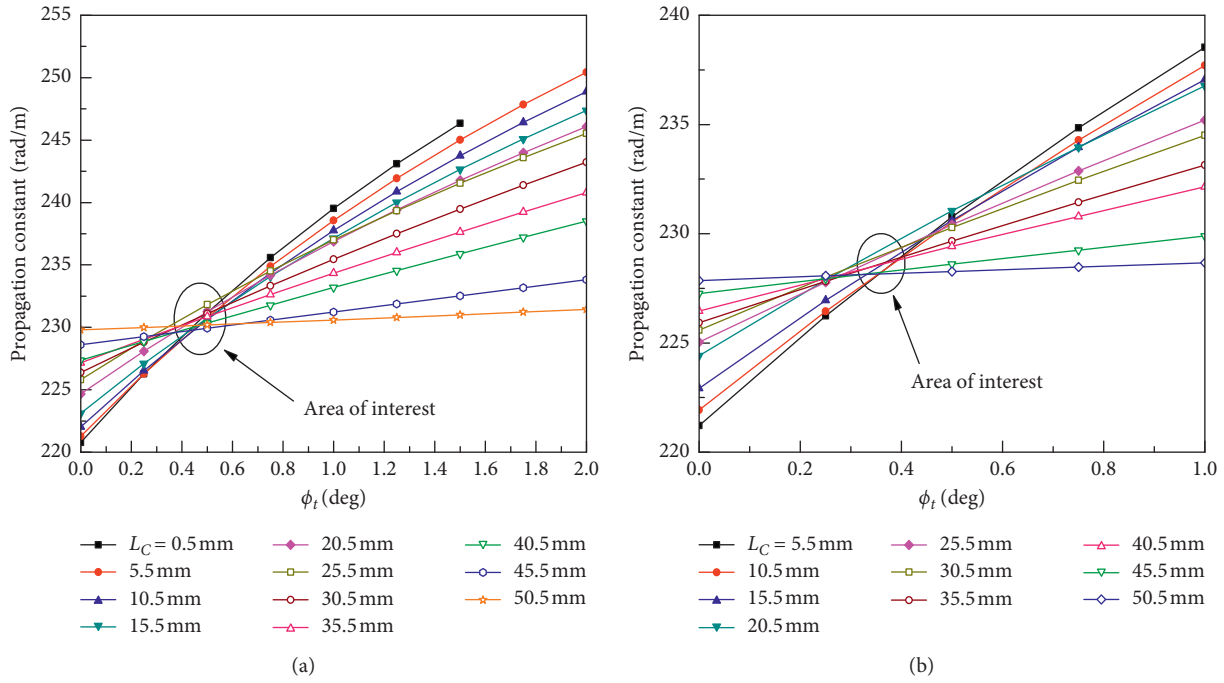

Figure 3: Wave propagation characteristics of conformal SIW along distance, L_C, and tilted width, $W(\phi)$ (Figure 2(c)): (a) cylindrical; (b) nose-cone.

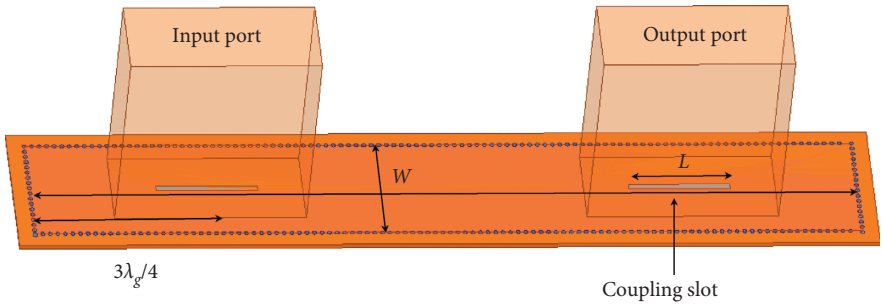

Figure 4: A scheme in which a rectangular waveguides (RWGs) are used to excite and observe field pattern of substrate-integrated waveguide (SIW).

conformed SIW, which is equal to two guided-wavelength, $2\lambda_g$. Whereas the tapering of via-holes along the longitudinal direction increases the width of SIW at the base (near to r_1) as shown in Figure 2(b). A new variable $W(\phi)$ is introduced, shown in Figure 2(c), while keeping the width of SIW fixed at the vertex of the cone and the arrays of conducting via holes are being tilted as shown in Figure 2(c). The simulated data of geometrical variables such as ϕ_t, L_C and β have been analyzed in Figure 3(b), and it is noted that the region of convergence of β_n curves is little bit expanded compared to the cylindrical case (Figure 3(a)). The vias of conformal SIW are tilted outward as shown in Figure 2(c); therefore, the width $W(\phi) > \lambda_0/2$.

4. Design of Conformal SIW Slotted Array

This section describes the steps involved in the designing of nose-cone conformal SIW slot array including feeding structure.

4.1. Array Feeding. To excite the array, two feeding techniques are considered: the first one is microstrip to SIW feeding and the second one is RWG to SIW feeding. The first technique is relatively easy to fabricate as the flexible substrate can be conformed comfortably to a predefined surface [27]. However, this could cause spurious radiations, which can possibly affect the overall performance of the system [6].

RWG to SIW feeding is a better option if adopted for conformal array design. One major advantage of RWG to SIW feed is that it suppresses spurious radiations. The half cosine incident wave will intersect with the lower coupling slot of SIW and can be tuned by off-setting from the center. The coupling slot is similar to the radiating slot [22], and it is located on SIW where the magnetic field is maximum. This kind of technique was utilized in [28] where the authors designed SIW slot array antenna on a cylindrical platform. They utilized RWG to SIW feed structure to excite 1×6 elements slot array. Their simulation results

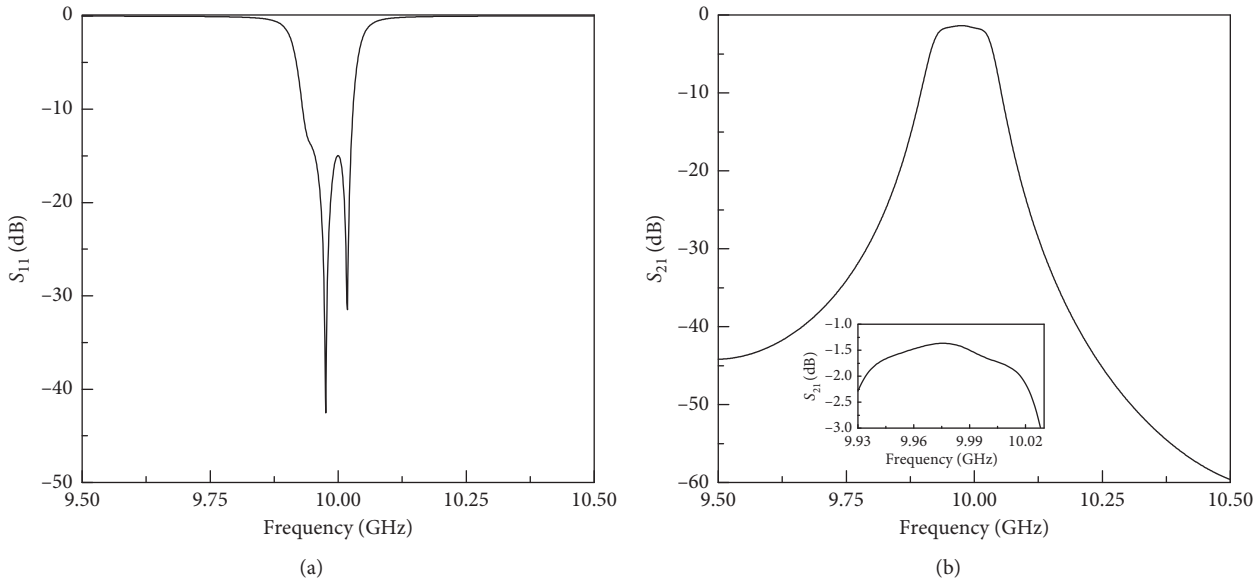

Figure 5: S-parameters of RWG to SIW feeding structure: (a) reflection parameter and (b) insertion loss; the inset of Figure 5(b) represents a zoomed view of region of interest.

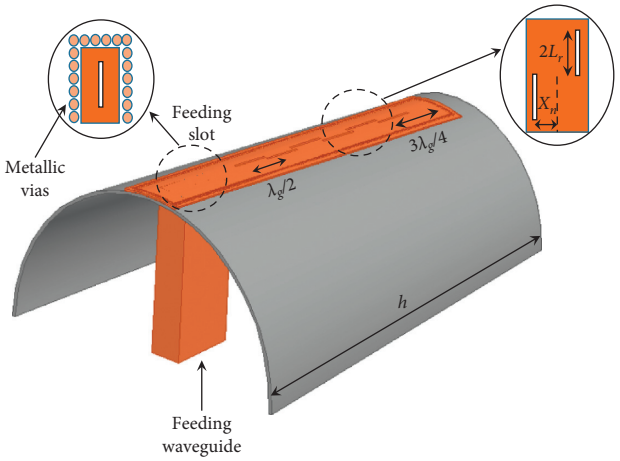

Figure 6: Configuration of hollow nose-cone conformal SIW slot array antenna.

Table 1: Design parameters of nose-cone and cylindrical conformal SIW slot array antennas.

Nose-cone parameters	Values	Cylinder parameters	Values
r_1 (mm)	$5\lambda_0$	r (mm)	$1.66\lambda_0$
r_2 (mm)	$4\lambda_0$	L_C (mm)	$5\lambda_0$
L_C (mm)	$5\lambda_0$	L_{CSIW} (mm)	$5\lambda_g$
L_{CoSIW} (mm)	$5\lambda_g$	W (mm)	$\lambda_0/2$

Table 2: Slot parameters for nose-cone conformal antenna with interelement spacing of $\lambda_g/2$.

S. No.	X_n (mm)	$2L_r$ (mm)
1	0.630	11.333
2	0.858	11.515
3	0.974	11.583
4	0.980	11.591
5	0.875	11.508
6	0.672	11.290

showed that the presented array had SLL of −21.72 dB with a gain of 9.8 dBi.

Figure 4 illustrates RWG to SIW feeding structure. From the figure, it can be observed that two coupling slots are placed on SIW structure. The distance from the center of the slot to conducting vias is $3\lambda_g/4$ as shown in Figure 4. Two rectangular waveguides represented as input and output ports are used to calculate the power transfer characteristics from one port to another.

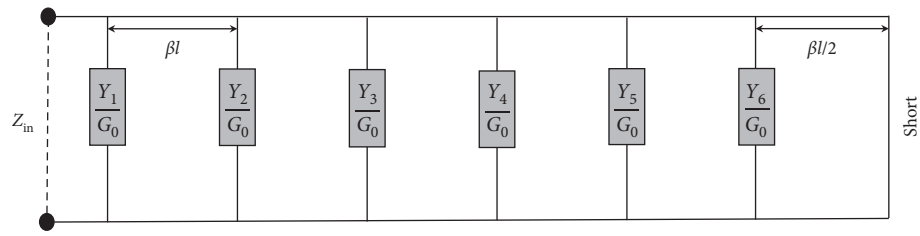

Figure 7: Equivalent circuit model of slotted array.

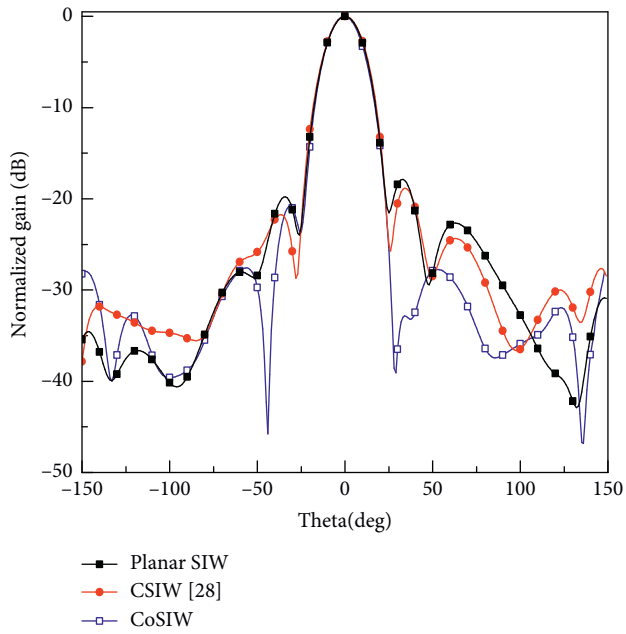

Figure 8: H-plane radiation characteristics of planar, cylindrical, and nose-cone conformal slot arrays.

Table 3: Comparative analysis for planar, cylindrical, and nose-cone conformal SIW slot arrays ($N = 6$ and $d = \lambda_g/2$).

Parameters	Planar SIW	Cylindrical SIW [28]	Nose-cone SIW
1st SLL (dB)	−19.78	−21.72	−20.82
2nd SLL (dB)	−17.85	−18.83	−27.63
SIW tilt (deg)	0°	0°	0.43°
Beam position (deg)	0°	0°	0°
HPBW (deg)	20.29°	21.24°	19.80°
Max. gain (dBi)	9.36	9.8	11.91

The S-parameters of RWG to SIW feeding structure are shown in Figure 5. It can be observed from Figure 5(a) that the proposed feeding technique is operating well for the frequency of interest, which is 10 GHz. Therefore, from Figure 5(a), it can be noted that the proposed feeding structure provides 100 MHz bandwidth from 9.93 to 10.03 GHz. The reason behind such a narrow bandwidth is that the conducting vias are tightly spaced, which tend to cause electric field leakage. The dielectric losses could be another reason for the observed narrow bandwidth for the proposed feeding structure [29]. On the other hand, the broadband transition, such as reported in [30], cannot be implemented directly in the proposed design, because it is difficult to conform E-plane iris of RWG on the nose-cone surface.

Figure 5(b) shows the insertion loss of the proposed feeding structure. From the figure, it is observed that the variation in insertion transition is 1.25 dB, which could primarily be associated with dielectric losses of the medium [29] and coupling losses of both the ports of the proposed design.

4.2. Array Design and Simulation. The graphical view of longitudinal slot array on the nose-cone surface is represented in Figure 6. It is pertinent to mention here that a hollow conical surface has been selected for the proposed design. Moreover, substrate chosen for the design of slotted array is Rogers RT/Duroid 5880 having $h = 0.508$ mm,

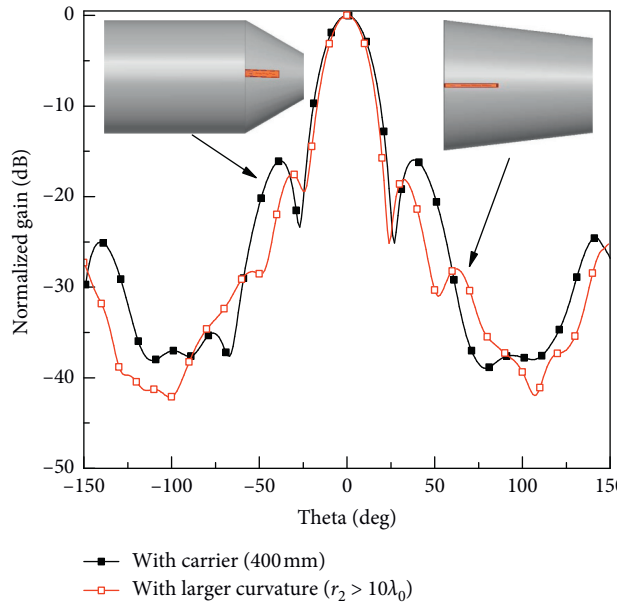

Figure 9: Effect of large curvature and carrier surface on antenna's radiation characteristics.

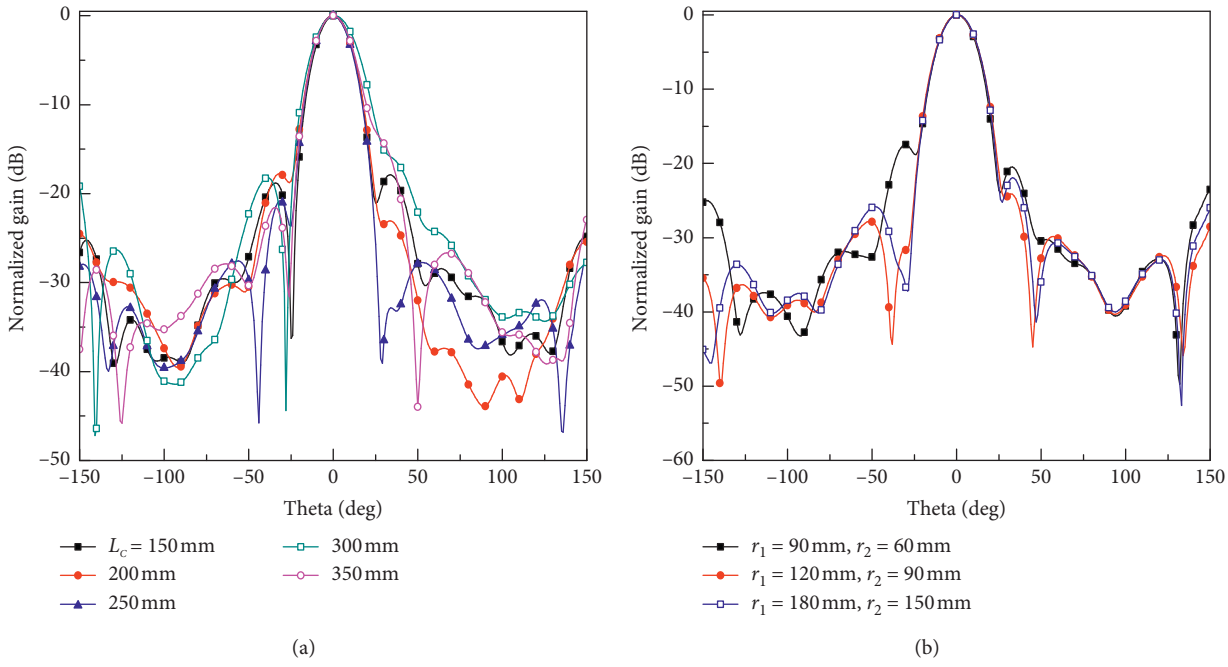

Figure 10: Effect of nose-cone parameters (a) L_C and (b) r_1 and r_2 on antenna's performance.

$\varepsilon_r = 2.2$, and $\tan\delta = 0.0009$. The center frequency of the designed array is 10 GHz. The array is projected on the conical surface of lower radius, r_1 and upper radius, r_2 as shown in Figure 2(b), while the width W of the nose-cone conformal SIW is selected according to the process defined in Section 3. The diameter of the metal vias is 0.5 mm, and the separation between them is 0.9 mm. The rest of the design parameters are listed in Table 1. This table provides variables for two different designs: one deals with the proposed nose-cone design listed in column 1, whereas for comparison purposes, cylindrical design parameters are also provided in the table.

The road map for the designed array is the same as that of Elliot's design technique [20, 24]. To get optimum radiation characteristics with low SLL, the slot offsets and their corresponding lengths, listed in Table 2, are obtained by using the method of least square (MLS) [4, 10]. The error function, which is used for pattern synthesis is given in equation (6) [4]:

(a) (b)

Figure 11: Prototype of the fabricated nose-cone conformal slot array antenna. (a) Slotted array conformed on conical platform. (b) Rectangular waveguide with SMA connector.

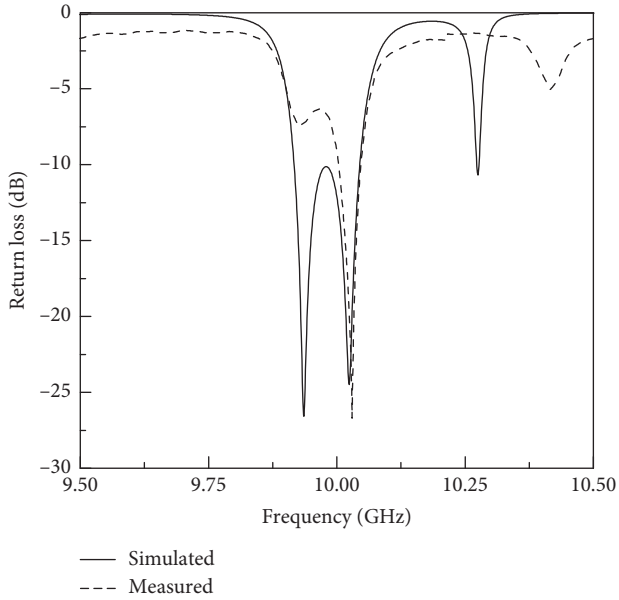

Figure 12: Return loss characteristics of the proposed nose-cone conformal slot array.

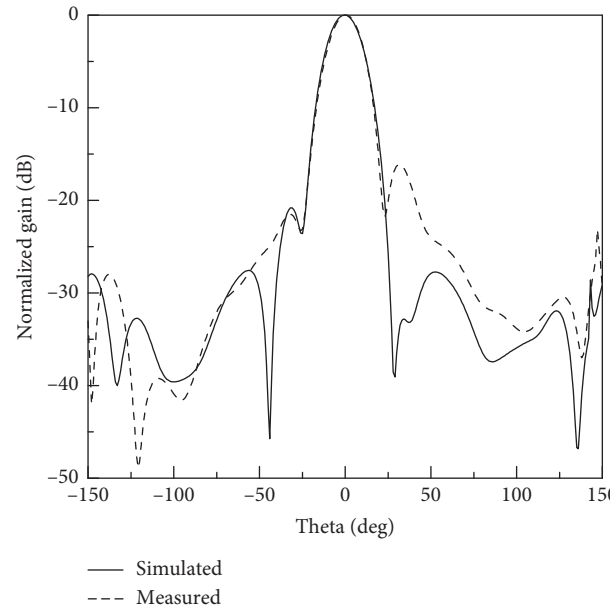

Figure 13: H-plane radiation characteristics of the proposed nose-cone conformal slot array.

$$\varepsilon_{\text{syn}} = W^{\text{upper}} \sum_{m=1}^{M} \left| S(\theta_m) - h_m^{\text{upper}} \right| + W^{\text{lower}} \sum_{m=1}^{M} \left| S(\theta_m) - h_m^{\text{lower}} \right|, \tag{6}$$

where W^{upper} and W^{lower} are the weights, while h_m^{upper} and h_m^{lower} represent upper and lower limits of SLL, respectively; $S(\theta_m)$ denotes array factor and M represents maximum number of iterations.

Once the conformal SIW slot array is designed, then its equivalent circuit model can be implemented by the classical slot array theory [23] as shown in Figure 7. Wherein the inter element spacing is $\lambda_g/2$, Y represents admittance of the elements, G_0 is the normalized conductance of slots, Z_{in} is the input impedance of the array, and the array is short circuited at $3\lambda_g/4$.

The proposed nose-cone conformal SIW slot array antenna is validated by comparing its radiation characteristics, shown in Figure 8, with planar and cylindrical conformal [28] SIW slot arrays. From the figure, it can be observed that the radiation characteristics are almost the same for all the three cases, but nose-cone conformal array provides low SLLs, which could be considered as a major achievement of nose-cone conformal design. From Figure 8, it can also be observed that the arrays have the main beam position in the

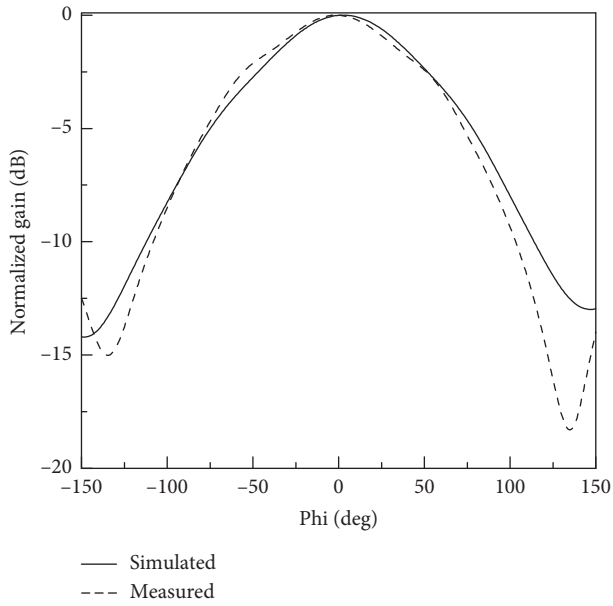

Figure 14: E-plane radiation characteristics of the proposed nose-cone conformal slot array.

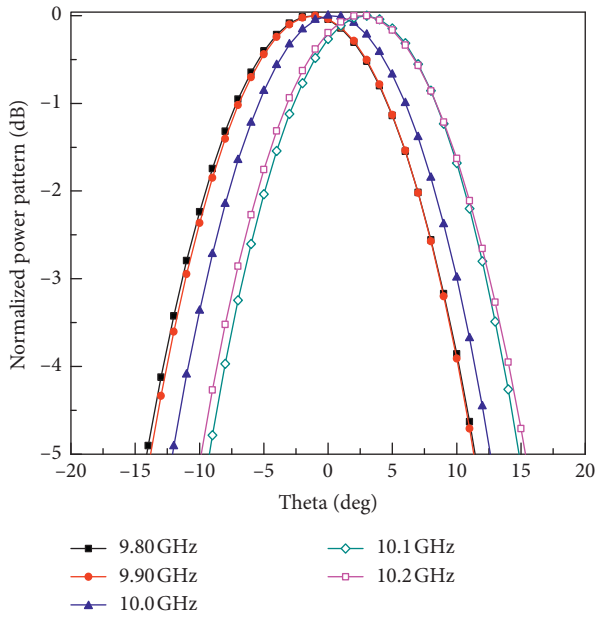

Figure 15: Main beam positioning vs. frequency.

broadside direction ($\theta = 0^{\circ}$). Different electrical parameters of all the three distinct surfaces are listed in Table 3, where the comparative analysis for the presented cases is given.

In nose-cone conformal case, the 1st SLL, given in Table 3, is equal to −20.82 dB, while the 2nd SLL is equal to −27.63 dB. Such low values of SLL could possibly be associated with the conformity of the radiating array with the supporting surface. The maximum gain of the nose-cone conformal slot array antenna at 10 GHz is 11.91 dBi, while the half power beam width (HPBW) is 19.80°. The maximum gain values for planar and cylindrical conformal arrays are 9.36 dBi and 9.8 dBi, respectively; as listed in Table 3. In nutshell, it can be claimed that nose-cone conformal SIW array antenna provides better gain and low SLLs.

Figure 9 shows the effect of large curvature and carrier surface on antenna's performance. It has been observed from Figure 9 that if the curvature of the nose-cone is increased as large as $10\lambda_0$, then the effect of conformity tends to be minimum and the surface will behave as a planar surface [16]. Accordingly, the radiation pattern due to the large curvature of the nose-cone conformal antenna is approximately equal to planar antenna as shown in Figure 9. On the other hand, when nose-cone conformal antenna is embedded with carrier surface, shown in inset of Figure 9, an increase in SLLs and beamwidth has been observed. This is due to the fact that the carrier surface provides extra reflections at the edges of nose-cone conformal antenna.

Figure 10(a) shows the simulated radiation patterns for different values of L_C. It has been noted from the figure that, for $L_C = 150$–250 mm, the SLLs are reducing. For values >250 mm, the SLLs increases with the spread in the main beam up to some extent as shown in Figure 10(a).

The effect of r_1 and r_2 on antenna's performance is illustrated in Figure 10(b). From the figure, it has been observed that SLLs tend to reduce with the increase in r_1 and r_2 value, while the gain variation is about 0.5 dB.

4.3. Fabrication and Measurements. The prototype of the proposed nose-cone conformal SIW slot array antenna is shown in Figure 11. Four major steps are involved in the fabrication of the proposed antenna array. First, fabrication of SIW is performed, which involves the etching of slot elements, drilling, and metallization of via holes. Second, a cone is fabricated in accordance with the design parameters listed in Table 1 by using a metallic sheet of thickness 14 AWG as shown in Figure 11(a). Third, RWG (WR-90) having one end compatible to the conical surface is attached to the inner surface of the cone through a machined window as shown in Figure 11(b), while an SMA connector is inserted at a distance of $\lambda_g/4$ from shorted end of a waveguide. The last step is to wrap SIW slot array on the conical surface to excite the array by feeding slot.

The return loss characteristics of the fabricated antenna are measured using the vector network analyzer (VNA) and compared with the simulated results. From Figure 12, a reasonable match is observed between simulated and measured return loss. An acceptable match between simulated and measured results validate the proposed nose-cone SIW design. Some discrepancies are observed between the simulated and measured return losses, which could be associated with the fabrication tolerances especially the mounting of RWG on conical platform.

In Figures 13 and 14, a comparison between simulated and measured H-plane and E-plane radiation patterns is shown for the proposed nose-cone conformal SIW slot array. For H-plane, shown in Figure 13, the simulated results offer SLLs of −20.82 dB and −27.63 dB, respectively; while the measured SLLs are −20.82 dB and −16 dB, respectively. An obvious reason of the observed discrepancy could be that the feeding part of the

Table 4: Comparative study of proposed and previously presented antenna arrays.

Parameters	[25]	Proposed
Array size	1×8	1×6
Cone type	Solid cone	Hollow nose-cone
Waveguide type	Wire-cut waveguide	Suspended waveguide
Design procedure	β and Z_{in} optimization on cylindrical surface	β optimization on conical surface
Return loss	>-10 dB	<-10 dB
Gain	9.9 dBi	11.91 dBi

conformed array is located at the base of hollow nose-cone as shown in Figure 11(b), and a mismatch between RWG and SIW, because of its tapered nature, caused an extra reflection, and hence increased the SLL, which ultimately degrades radiation characteristics of the proposed antenna. On the other hand, the designed antenna consists of only one row of radiating slots; therefore, its radiation characteristics are deteriorated in the E-plane by the fixed screw blockage and the lateral size of an SIW slot array antenna as shown in Figure 14. Furthermore, the proposed antenna provides linear polarization and radiation efficiency of 70%.

By using the proposed nose-cone conformal SIW array antenna, the main beam can be steered by changing the frequency to increase the coverage. The patterns thus achieved indicating the position of main beam as a function of frequency are shown in Figure 15.

A comparative analysis between proposed and previously presented conformal arrays is given in Table 4. By examining the values of return loss and the gain as shown in the table, it can be noted that the proposed array has better performance than the design presented in [25]. It is worth mentioning here that the proposed nose-cone conformal array offers high gain even with less number of elements.

5. Conclusion

This paper presents the design of X-band nose-cone conformal substrate-integrated waveguide longitudinal slot array antenna. The wave propagation on nose-cone has been investigated, and a rectification process has been proposed through EM simulations. The simulated radiation characteristics of the proposed array are compared with planar and cylindrical conformal arrays, and it is observed that the proposed nose-cone conformal array offers relatively high gain with low SLLs. Furthermore, the nose-cone conformal array is validated through fabrication and a good agreement is observed between the measured and the simulated data. The presented study demonstrate that the proposed antenna array can be utilized in modern radars and on the conical surface of aircrafts and missiles.

Data Availability

The data used to support the findings of this study are available from the corresponding author upon request.

Conflicts of Interest

The authors declare that there are no conflicts of interest regarding the publication of this paper.

References

[1] S. W. Schneider, C. Bozada, R. Dettmer, and J. Tenbarge, "Enabling technologies for future structurally integrated conformal apertures," in *Proceedings of the IEEE Antennas and Propagation Society International Symposium. Held in Conjunction with: USNC/URSI National Radio Science Meeting*, vol. 2, pp. 330–333, Boston, MA, USA, July 2001.

[2] D. Wingert and B. Howard, "Potential impact of smart electromagnetic antennas on aircraft performance and design," in *Proceedings of the NATO Workshop on Smart Electromagnetic Antenna Structures*, pp. 1–10, Brussels, Belgium, November 1996.

[3] R. J. Mailloux, *Conformal Array Antenna Theory and Design (Reviews and Abstracts)*, Wiley-Interscience Publication, Hoboken, NJ, USA, 2007.

[4] S. E. Hosseininejad and N. Komjani, "Optimum design of traveling-wave SIW slot array antennas," *IEEE Transactions on Antennas and Propagation*, vol. 61, no. 4, pp. 1971–1975, 2012.

[5] D. Deslandes, "Design equations for tapered microstrip-to-substrate integrated waveguide transitions," in *Proceedings of the 2010 IEEE MTT-S International Microwave Symposium*, pp. 704–707, Anaheim, CA, USA, May 2010.

[6] M. I. Nawaz, Z. Huiling, and M. Kashif, "Substrate integrated waveguide (SIW) to microstrip transition at X-band," in *Proceedings of the 2014 International Conference on Circuits, Systems and Control*, pp. 61–63, Yueyang, China, June 2014.

[7] M. Bozzi, F. Xu, D. Deslandes, and K. Wu, "Modeling and design considerations for substrate integrated waveguide circuits and components," in *Proceedings of the 8th International Conference on Telecommunications in Modern Satellite, Cable and Broadcasting Services*, pp. 7–16, Nis, Serbia, September 2007.

[8] D. Deslandes and K. Wu, "Integrated microstrip and rectangular waveguide in planar form," *IEEE Microwave and Wireless Components Letters*, vol. 11, no. 2, pp. 68–70, 2001.

[9] J. Wu, Y. J. Cheng, and Y. Fan, "A wideband high-gain high-efficiency hybrid integrated plate array antenna for V-band inter-satellite links," *IEEE Transactions on Antennas and Propagation*, vol. 63, no. 4, pp. 1225–1233, 2015.

[10] S. E. Hosseininejad, N. Komjani, and A. Mohammadi, "Accurate design of planar slotted SIW array antennas," *IEEE Antennas and Wireless Propagation Letters*, vol. 14, pp. 261–264, 2015.

[11] J. Dong, Y. Wang, F. Meng, and W. Feng, "A research on airborne conformal array with high gain and low SLL," in *Proceedings of the 2014 International Conference on Computational Intelligence and Communication Networks*, pp. 334–338, Bhopal, India, November 2014.

[12] A. Traille, J. Ratner, G. D. Hopkins, and V. Tripp, "Development of a novel faceted, conformal, slotted-waveguide subarray for sensor applications with full 360° azimuth tracking capabilities," in *Proceedings of the 2007 IEEE*

Antennas and Propagation Society International Symposium, pp. 3828–3831, Honolulu, HI, USA, June 2007.

[13] O. Bayraktar and O. A. Civi, "Circumferential traveling wave slot array on cylindrical substrate integrated waveguide (CSIW)," *IEEE Transactions on Antennas and Propagation*, vol. 62, no. 7, pp. 3557–3566, 2014.

[14] Y. Y. Liu, M. Guo, and S. S. Zhong, "Conformal slotted waveguide array antenna," in *Proceedings of the 2012 IEEE International Workshop on Antenna Technology (iWAT)*, pp. 56–59, Tucson, AZ, USA, March 2012.

[15] P. Chopra, M. Bhandari, and S. Saxena, "Conformal antenna using circular microstrip patches in C band," in *Proceedings of the 3rd International Conference on Signal Processing and Integrated Networks (SPIN)*, pp. 759–762, Noida, India, February 2016.

[16] H. Yang, Z. Jin, G. Montisci et al., "Design equations for cylindrically conformal arrays of longitudinal slots," *IEEE Transactions on Antennas and Propagation*, vol. 64, no. 1, pp. 80–88, 2016.

[17] P. Knott, C. Loker, and S. Algermissen, "Antenna element design for a conformal antenna array demonstrator," in *Proceedings of the 2011 Aerospace Conference*, pp. 1–5, Big Sky, MT, USA, March 2011.

[18] T. Pelham, G. Hilton, E. Mellios, and R. Lewis, "Predicting conformal aperture gain from 3-D aperture and platform models," *IEEE Antennas and Wireless Propagation Letters*, vol. 16, pp. 700–703, 2017.

[19] A. K. Aboul-Seoud, A. D. S. Hafez, A. M. Hamed, and M. Abd-El-Latif, "A conformal conical phased array antenna for modern radars," in *Proceedings of the 2014 IEEE Aerospace Conference*, pp. 1–7, Big Sky, MT, USA, March 2014.

[20] R. Elliott and L. Kurtz, "The design of small slot arrays," *IEEE Transactions on Antennas and Propagation*, vol. 26, no. 2, pp. 214–219, 1978.

[21] R. Elliott and W. O'Loughlin, "The design of slot arrays including internal mutual coupling," *IEEE Transactions on Antennas and Propagation*, vol. 34, no. 9, pp. 1149–1154, 1986.

[22] M. Orefice and R. S. Elliott, "Design of waveguide-fed series slot arrays," *IEE Proceedings H Microwaves, Optics and Antennas*, vol. 129, no. 4, pp. 165–169, 1982.

[23] R. S. Elliot, *Antenna Theory and Design*, John Wiley & Sons, Hoboken, NJ, USA, 2006.

[24] R. Elliott, "An improved design procedure for small arrays of shunt slots," *IEEE Transactions on Antennas and Propagation*, vol. 31, no. 1, pp. 48–53, 1983.

[25] Y. F. Wu and Y. J. Cheng, "Conical conformal shaped-beam substrate-integrated waveguide slot array antenna with conical-to-cylindrical transition," *IEEE Transactions on Antennas and Propagation*, vol. 65, no. 8, pp. 4048–4056, 2017.

[26] R. Harrington, *Time-Harmonic Electromagnetic Fields, IEEE Press Series on Electromagnetic Wave Theory*, Wiley, Hoboken, NJ, USA, 2001.

[27] L. Li, X. Chen, R. Khazaka, and K. Wu, "A transition from substrate integrated waveguide (SIW) to rectangular waveguide," in *Proceedings of the 2009 Asia Pacific Microwave Conference*, pp. 2605–2608, Singapore, December 2009.

[28] H. Khalil, M. M. Ahmed, U. Rafique, Saeed-ur-Rehman, M. Latif, and W. Nazar, "Design of X-band cylindrical conformal substrate integrated waveguide slot antenna array," in *Proceedings of the 2018 21st Saudi Computer Society National Computer Conference (NCC)*, pp. 1–4, Riyadh, Saudi Arabia, April 2018.

[29] A. Rhbanou, S. Bri, and M. Sabbane, "Analysis of substrate integrated waveguide (SIW) resonator and design of miniaturized SIW bandpass filter," *International Journal of Electronics and Telecommunications*, vol. 63, no. 3, pp. 255–260, 2017.

[30] R. Vincenti Gatti, R. Rossi, and M. Dionigi, "Broadband right-angle rectangular waveguide to substrate integrated waveguide transition with distributed impedance matching network," *Applied Sciences*, vol. 9, pp. 1–16, 2019.